International Journal of Applied Earth Observation and Geoinformation 58 (2017) 26–35

Contents lists available at ScienceDirect

International Journal of Applied Earth Observation and Geoinformation

journal homepage: www.elsevier.com/locate/jag

Quantification of dead vegetation fraction in mixed pastures using AisaFENIX imaging spectroscopy data

R.R. Pullanagari*, G. Kereszturi, I.J. Yule

New Zealand Centre for Precision Agriculture, Department of Soil and Earth Sciences, Institute of Agriculture and Environment (IAE), Massey University, Palmerston North, Private Bag 11-222, New Zealand

ARTICLE INFO

Article history:
Received 18 September 2015
Received in revised form 29 February 2016
Accepted 11 January 2017
Available online 5 February 2017

Keywords:
Pasture
Imaging spectroscopy
Dead vegetation
NDVI
Partial least squares

ABSTRACT

New Zealand farming relies heavily on grazed pasture for feeding livestock; therefore it is important to provide high quality palatable grass in order to maintain profitable and sustainable grassland management. The presence of non-photosynthetic vegetation (NPV) such as dead vegetation in pastures severely limits the quality and productivity of pastures. Quantifying the fraction of dead vegetation in mixed pastures is a great challenge even with remote sensing approaches. In this study, a high spatial resolution with pixel resolution of 1 m and spectral resolution of 3.5–5.6 nm imaging spectroscopy data from AisaFENIX (380–2500 nm) was used to assess the fraction of dead vegetation component in mixed pastures on a hill country farm in New Zealand. We used different methods to retrieve dead vegetation fraction from the spectra; narrow band vegetation indices, full spectrum based partial least squares (PLS) regression and feature selection based PLS regression. Among all approaches, feature selection based PLS model exhibited better performance in terms of prediction accuracy (R^2_{CV} = 0.73, $RMSE_{CV}$ = 6.05, RPD_{CV} = 2.25). The results were consistent with validation data, and also performed well on the external test data (R^2 = 0.62, RMSE = 8.06, RPD = 2.06). In addition, statistical tests were conducted to ascertain the effect of topographical variables such as slope and aspect on the accumulation of the dead vegetation fraction. Steep slopes (>25°) had a significantly ($p < 0.05$) higher amount of dead vegetation. In contrast, aspect showed non-significant impact on dead vegetation accumulation. The results from the study indicate that AisaFENIX imaging spectroscopy data could be a useful tool for mapping the dead vegetation fraction accurately.

1. Introduction

Grazed pasture is the main source of livestock feed because it is a cheap feed source, and available throughout the year. Pasture quality has a direct effect on feed intake and animal performance, and is strongly determined by the content of legumes, leaves, stems and non-photosynthetic vegetation (NPV) such as dead vegetation (Holmes et al., 2007). The accumulation of dead vegetation can be attributed to a number of factors including; under grazing and older tissue lost through senescence and decomposition. Variable rainfall events (Guerschman et al., 2009) and availability of soil moisture is also critical for pasture growth as dead vegetation accumulation is greater under dry conditions. In addition, local scale spatial variability caused by environmental factors such as soil type and fertility affects the proportion of dead vegetation. On hill country sheep and beef farms the variability is further complicated by topographic variables such as slope and aspect, and nutrient return by animals (Gillingham, 1973; Zhang et al., 2004). For instance, steep and south-facing slopes in hill country pastures have a considerable proportion of dead vegetation due to low soil moisture and high temperature (Gillingham, 1973). The feed value of pasture decreases as the proportion of dead material accumulation increases and animals avoid these areas (White and Hodgson, 2000). It should be noted that facial eczema fungus thrives well on dead material in mixed pastures. The spores of the fungus release toxins including zearalenone and trichothecenes, which affect animal performance and depresses ovulation rates in ewes (Keogh, 1986; Morris et al., 2004). Therefore, it is necessary to quantify the dead vegetation fraction accurately so that pastures can be managed with greater precision.

During the last few decades, grassland remote sensing has evolved and developed to include; vegetation monitoring, mapping of biophysical (e.g., biomass and leaf area index) and biochemical attributes (e.g., nitrogen, phosphorus, fibre) (Knox et al., 2011; Pullanagari et al., 2012; Ren et al., 2012), mapping of weed infesta-

* Corresponding author.
E-mail addresses: P.R.Reddy@massey.ac.nz, shekerreddy@hotmail.com (R.R. Pullanagari).

http://dx.doi.org/10.1016/j.jag.2017.01.004
1569-8432/

tion and fraction of vegetation cover (Hestir et al., 2008). Vegetation distribution maps and prediction models developed from remote sensing images allow us to understand the underlying mechanisms responsible for vegetation changes in different ecosystems. Airborne and spaceborne optical sensors enable us to monitor vegetation health over large areas in a time series fashion, and provide spatially explicit information. Many efforts have been made to estimate NPV, particularly crop residue and plant litter where green vegetation can be absent or present in small proportions. However, limited research has been conducted to estimate NPV in the presence of mixed environment, particularly in grazed pastures (Numata et al., 2008; Ren and Zhou, 2012; Xu et al., 2014; Yang and Guo, 2014). In remote sensing, two main approaches have widely been used to estimate the NPV. Firstly, a number of empirical relationships have been developed between spectral indices and fraction of NPV. These indices were further divided into multispectral and hyperspectral indices based on the spectral resolution of the sensors. Multispectral indices such as normalized difference senescent vegetation index (NDSVI) (Qi et al., 2002), normalized difference vegetation index (NDVI) (Xu et al., 2014), and normalized difference index (NDI) (McNairn and Protz, 1993) were developed for estimating NPV in different ecosystems. However, multispectral indices could not account for the narrow spectral features of dead vegetation due to their broad spectral resolution resulting in unreliable estimations (Numata et al., 2008; Daughtry et al., 2010; Guerschman et al., 2009). Ren et al. (2012) proved that vegetation indices from Landsat 7 TM produced unreliable estimates for senesced biomass in the desert steppe of Inner Mongolia. In addition, multispectral sensors such as Landsat 8 and Spot 4 are designed to have bands in visible and near infrared regions where dead vegetation has similar or confounding optical features with bare soil, moss and lichen (Daughtry, 2001; Qi and Wallace, 2002; Ustin et al., 2009), thus a poor relationship can be expected. Moreover, this spectral ambiguity is more pronounced when the leaf area index (LAI) is low (Delegido et al., 2015). Theoretically, NPV has high cellulose and lignin content compared to green vegetation and is absent in soil (Asner et al., 2003). These difference cause variations in their spectra. Utilizing these differences, numerous hyperspectral indices have been proposed based on the absorption features of cellulose and lignin present in the short wave infrared (SWIR) region of the spectrum. Daughtry et al. (1996) designed a cellulose absorption index (CAI) based on the relative depth of the absorption features occurring in the 2000–2200 nm for discriminating plant litter from soil. Numata et al. (2008) used the spectral features ligno-cellulose absorption depth (LCD) and lingo-cellulose absorption area (LCA) between 2045 and 2218 nm for estimating senesced biomass of grazed pastures in Rondônia in the Brazilian Amazon. Delegido et al. (2015) identified a new hyperspectral NDI with a band combination of 2154 and 1635 nm for mapping the LAI of senescent vegetation of field crops at the agricultural site in Barrax, Spain. However, the performance of these indices was influenced by the presence of green vegetation and soil mineralogy in the spectra (Li and Guo, 2015). The CAI has less sensitivity to crop residue estimation when the fraction of green vegetation presents more than 30% (Daughtry et al., 2004).

The second approach for estimating NPV cover is spectral unmixing using the spectral features present in the SWIR. Asner et al. (2003) used a linear spectral unmixing approach for mapping the fractions of green and dead vegetation, and bare soil in arid and semiarid forest regions using the spectral features present in the SWIR region. Nonetheless, all of the above methods are not suitable for an accurate quantitative evaluation of NPV, and their application severely limits the water content in vegetation and presence of high green vegetation fraction (Li and Guo, 2015). Conversely, a full range hyperspectral sensor has the potential to quantify the fraction of dead vegetation because of the presence of visible near infrared (Vis-NIR) and SWIR bands as it contains sufficient information regarding the sensitivity to changes in the proportion of dead vegetation (Numata et al., 2008; Ren and Zhou, 2012; Xu et al., 2014). Moreover, hyperspectral sensors collects the information in narrow and contiguous bands, which enhances the qualitative and quantitative ability of vegetation attributes (Knox et al., 2011; Landmann et al., 2015; Pullanagari et al., 2012; Skidmore et al., 2010). Airborne imaging spectroscopy or hyperspectral imaging creates an opportunity to evaluate the potential for mapping the dead vegetation fraction at a range of spatial scales and to monitor temporal variations.

The objective of this research was to quantify the dead vegetation fraction in grazed pasture using imaging spectroscopy (IS) data from the airborne AisaFENIX system. The relationship between the spectral data and the dead vegetation fraction was evaluated by different statistical methods, empirical models based on vegetation indices such as optimized narrowband vegetation indices using NDSVI, senescent vegetation index (SVI), cellulose absorption index (CAI), lingo-cellulose absorption indices, and multivariate models based on full spectrum and selected spectral regions of the spectrum. Using the best model a spatial map for the dead vegetation fraction was created at farm scale. In addition to the spectral study, the impact of terrain's slope angle and slope aspect on dead vegetation accumulation was investigated.

2. Materials and methods

2.1. Study area

The study was conducted on a hill country farm, part of Ohorea station, located North of Whanganui, New Zealand during the autumn season. We chose this season because dead vegetation accumulation is higher in the autumn and summer seasons. The farm has 600 ha of grazing land within an elevation range of 260–780 m and is comprised of slopes varying from rolling to steep. The average annual rainfall of the study area is 1300 mm (5 year average). A second experiment was also conducted on a hill country farm during autumn at Limestone downs station, Waikato, New Zealand. Both locations had mixed sward pasture systems dominated by rye grass (*Lolium perenne*) and clover (*Trifolium repens*), and a small proportion of brown top (*Agrostis capillaris* L.), dandelion (*Taraxacum officinale*), yorkshire fog (Holcus lanatus), buttercup (*Ranunculus* spp), chickweed (*Stellaria media*) and yarrow (*Achillea millefolium*).

2.2. Imaging spectroscopy data and processing

The airborne imaging system used in this study was AisaFENIX (Specim Ltd., Finland) which is a push broom type full spectrum sensor with field of view of 32.3° and instantaneous field of view of 0.084°. The spectral range of the sensor from visible to shortwave infrared (380–2500 nm) with a sampling distance of 3.5 nm in visible and near infrared region, and 5.6 nm in SWIR region producing a total of 448 spectral bands. The spectral images were collected on a clear day with no visible cloud cover with an airborne imager system. The first experiment was conducted on 30th April 2014 and a total of 18 flight lines were imaged to cover the whole study area between 10:35 and 11:35 (NZTM). The second experiment was conducted on 8th May 2014 with 21 flight lines.

Before the flight scan, boresight calibration was conducted of a known site to ensure sensor mounting alignment was correct. The raw data produced from AisaFENIX were radiometrically corrected using calibration coefficients with CaliGeo software supplied by Specim Ltd., Finland. Then the image was geocoded and orthorectified using 8 m spatial resolution Digital Elevation Model (DEM)

Table 1
Descriptive statistics of calibration and validation data sets of dead vegetation.

Calibration data (n = 165)			Validation data (n = 110)		
Mean	Std	CV	Mean	Std	CV
27.32	13.62	49.88	26.58	13.01	48.95

obtained from the Land Information New Zealand website (www.linz.govt.nz) in conjunction with flight parameters such as GPS position, roll, pitch, heading and yaw angles. The image radiance values were then converted into surface reflectance values using ATCOR-4 (Richter and Schläpfer, 2014) which is based on the MODTRAN 5.3 radiative transfer code. The reflectance strips were mosaicked in order to obtain a single data cube, and subsequently spatially smoothed by a median filter with a pixel window of 3×3.

2.3. Ground data

Following the flight, a field work campaign was immediately conducted for ground sampling using a conventional agronomic method. These sampling sites were predetermined based on a stratified random design using the geographical information system (GIS) data layers of slope, aspect, soil type as well as farm accessibility. The sampling design ensured all the sampling sites were distributed in different classes of GIS data layers so that a high variability of dead vegetation could be expected. A total of 275 and 120 0.5×0.5 m size plots (Fig. 1b) were selected for analysis in first and second experiments, respectively. Within each plot, the proportion of dead plant material was visually estimated as a percentage of the total sward dry matter. The visual estimation was performed by an experienced observer and compared to calibrated photographs. The photographs were calibrated by measuring the harvested dead vegetation fraction. The sites were georeferenced with Real-Time Kinematic Global Positing System (RTK-GPS), thereby providing a geospatial accuracy of 5 cm.

2.4. Data analysis

Regions of interest (ROI) with a pixel window size of 3×3 centred over corresponding field sites were created. The average reflectance of each ROI was extracted and then used for further analysis. A series of pre-processing steps were executed on the spectra which include first derivative transformation applied using a Savitzky-Golay filter – window size 15, polynomial order 2 then followed by auto scaling.

In this study we adopted three approaches for developing a relationship between spectral data and reference values: (i) vegetation indices (ii) full-spectrum based partial least squares (PLS), and (iii) feature selection based PLS. The first experiment dataset ($n = 275$) was randomly divided into two datasets: 60% of the total samples ($n = 165$) were assigned to calibration and the remaining 40% were assigned to validation data ($n = 110$). The same amount of variation ensured for both data sets (Table 1). Calibration data was used for developing models which were then applied to the validation dataset for testing the model performance. In addition to validation, the second experiment data ($n = 120$) was used for testing the performance of the calibration model.

2.4.1. Vegetation indices (VI)

2.4.1.1. Optimized vegetation indices. Vegetation indices are the simple mathematical combination of reflectance values at different wavelengths which are used to regress against the attributes of vegetation using an appropriate fitted function. Hyperspectral data provides an opportunity to calculate many band combinations, hence we attempted to design all possible band combinations according to VI formulation. In this study we used NDSVI and senescent vegetation index (SVI) for calculating the optimal vegetation indices and their corresponding formulations presented below:

$$NDSVI_{a,b} = \frac{\rho_{\lambda(a)} - \rho_{\lambda(b)}}{\rho_{\lambda(a)} + \rho_{\lambda(b)}} \quad (1)$$

$$SVI_{a,b} = \frac{\rho_{\lambda(a)}}{\rho_{\lambda(b)}} \quad (2)$$

Where ρ is the derivative reflectance at the a^{th} or b^{th} wavelength (λ) which consists 448 bands in a spectral range from 380 to 2500 nm. After computing all possible band combinations, the resultant values were regressed against the dead vegetation fraction using linear fitting function. Best index bands were selected based on coefficient of determination (R^2) values. Jackknife cross-validation was performed which computes estimates by leaving out one observation at a time from the estimation sample (Abdi and Williams, 2010). The average R^2 value of n estimations was calculated. The relationships were then retested on the validation and the independent test.

2.4.1.2. Cellulose absorption index (CAI). The cellulose absorption index (CAI) was proposed by Daughtry et al. (1996) for detecting crop residue cover using absorption features caused by cellulose and lignin. CAI is computed using the following equation.

$$CAI = 100\,[0.5\,(\rho_{2000} + \rho_{2200}) - \rho_{2100}] \quad (3)$$

Where ρ_{2000}, ρ_{2200}, ρ_{2100} are the average reflectance values at 1997–2008 nm, 2196–2207 nm, 2097–2108 nm, respectively.

2.4.1.3. Ligno-cellulose absorption indices. Ligno-cellulose absorption indices were developed based on the absorption features of lignin and cellulose in the SWIR (Asner et al., 2003; Curran et al., 1997) which are capable of separating NPV from green vegetation and soil when the fraction of NPV is high (Numata et al., 2008). In this study, we used the continuum removal spectral range between 2040 and 2120 nm for calculating the absorption features such as band depth, band width and band area. The continuum removal technique normalizes the absorption features by drawing a straight line or convex hull over the local maxima points of the reflectance spectrum (Kokaly and Clark, 1999).

2.4.2. Full-spectrum partial least squares

The calibration model was developed using a PLS method where the variation present in both spectral data and measured data were used to construct a regression model. PLS reduces high dimensional spectral data into low dimensional data by generating new variables (also called PLS components) that link the $X_{n \times m}$ explanatory variables (spectral data) matrix to the $Y_{n \times 1}$ dead vegetation fraction vector by maximising the covariance between them (Wold et al., 2001). Initially, two external correlations were calculated for the X and Y matrices separately using eigenvalue decomposition as shown Eqs. (4) and (5).

$$X_{n \times m} = T_{n \times k} P'_{k \times m} + E_{n \times k} \quad (4)$$

$$Y_{n \times 1} = U_{n \times k} Q_{k \times 1} + F_{n \times 1} \quad (5)$$

Where $X_{n \times m}$ is a spectral data matrix of m wavebands and n samples, T is a matrix of X scores, P is a matrix of X loadings and E is a vector of residuals of the k^{th} PLS component of X. Concurrently, $Y_{n \times 1}$, $U_{n \times k}$, $Q_{k \times 1}$ and $F_{n \times 1}$ respectively stand for response variable vector, score matrix of Y, loading matrix of Y and vector of Y residuals. Next, the Nonlinear iterative partial least squares (NIPALS) algorithm was applied in order to construct an inner relation between X and Y and obtain a weight matrix $W_{m \times k}$ with

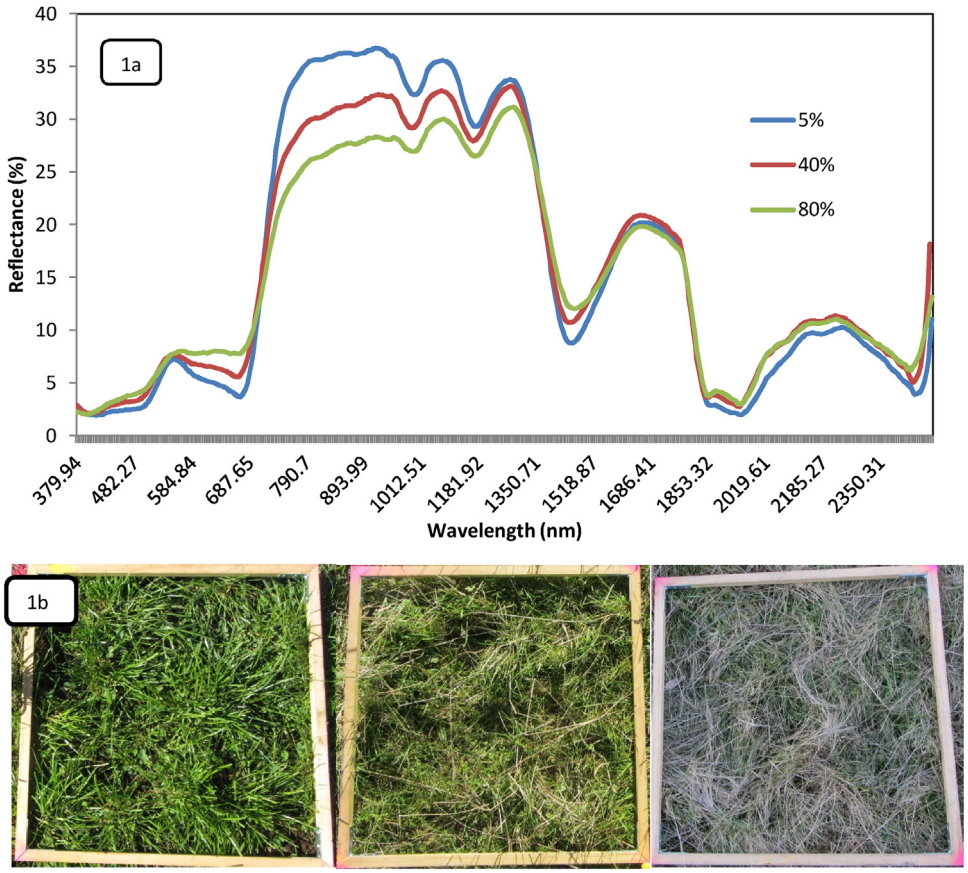

Fig. 1. (a) Reflectance of dead vegetation with different fractions derived from AisaFENIX imaging spectroscopy data, (b) Corresponding photos of vegetation samples with dead vegetation fractions of 5, 40, 80%.

the objective of minimising $\|F\|$ while maximising the covariance between the X and Y matrix (Eq. (6)).

$$U_{n\times k} = T_{n\times k} W_{m\times k} \tag{6}$$

The k^{th} PLS components are obtained ($k = 1, 2, \ldots h$) using the above equations. The extracted PLS components are orthogonal, and the number is optimised by performing the leave-one-out cross-validation. From this procedure, $RMSE_{CV}$ is calculated and used as a measure to select the optimal number of PLS components. In this, one sample at a time is left out and the PLS model is constructed with the remaining samples; the left out sample is then predicted and this procedure is repeated for each sample.

2.4.3. Feature selection based partial least squares

Interval partial least squares is a graphically oriented local regression modelling approach originally proposed by Norgaard et al. (2000). This technique focused on selecting important broad wavelength regions sensitive to dead vegetation changes and also highlighted the noisy regions. The spectrum was divided into a given number of equidistant subregions as intervals ($i = 20$), and then a PLS model was developed for each interval. In each interval 10 subsequent bands were considered as a single variable. The sensitive spectral regions were selected using the forward interval partial least squares (FiPLS) algorithm. Initially the algorithm was used where it selected the best interval at each time and subsequently added to the model until a maximum number of intervals ($i = 20$) was reached (Zou et al., 2007). $RMSE_{CV}$ was calculated for each interval using a PLS model. The interval with lowest $RMSE_{CV}$ is selected first then it again searches for a new interval showing the next lowest $RMSE_{CV}$. This was repeated until the maximum number of intervals was reached. In cross-validation, each interval was left out in turn and the root mean square error cross-validation ($RMSE_{CV}$) calculated for the remaining intervals (n-1) using a PLS model. FiPLS method is unlikely to find best single important wavelengths in the spectra (Andersen and Bro, 2010) hence, the selected intervals were further evaluated using variable importance projection (VIP) (Wold et al., 2001). VIP was calculated with the following equation:

$$VIP_m(k) = m\sum_k w_{km}^2 \left(\frac{SSY_k}{SSY_t}\right) \tag{7}$$

Where $VIP_m(k)$ is the value of m^{th} wavelength based on a PLS model with a factors, W_{km} represents PLS model weight of m^{th} wavelength in the k^{th} PLS factor, SSY_k is the explained sum of squares of dead vegetation content (Y) by a PLS model with a factors, SSY_t is the total sum of squares of Y explained in all a factors of a PLS model. The wavelengths with a VIP value > 1 were considered in the final model (Pullanagari et al., 2012).

The legitimacy of cross-validated calibration and test models was evaluated by coefficient of determination (R^2), root mean square error (RMSE) and ratio prediction to deviation (RPD). The reliability of the model prediction accuracy was validated using the independent test dataset obtained from the second experiment.

$$RPD = \frac{SD(y)}{\sqrt{\frac{\sum_{i=1}^{n}(\hat{y}_i - y_i)^2}{n}}} \tag{8}$$

Where n is the number of samples, $\hat{y}_i$ and y_i are the estimated and measured value of i^{th} sample, respectively. $SD(y)$ and $\bar{y}$ is the standard deviation and mean of the measured values (y).

In order to understand the impact of slope and aspect on accumulation of the dead vegetation fraction in mixed pasture, a statistical test has been conducted. In this study, the data does not meet the assumptions for one-way ANOVA so, Kruskal-Wallis one-way analysis by ranks was conducted (Siegel and Castellan, 1956). The significant differences were further evaluated by applying a post-hoc test for multiple comparisons (Giraudoux, 2012). The farm geographical area was divided into four categories based on slope angle (Zhang et al., 2004): (i) 0–8° (ii) 8–16° (iii) 16–25° (rolling to steep hill) (iv) 25°<(steep). The aspect classes included in the analysis are (i) North (ii) East (iii) South (iv) West. The slope angles and aspect values were calculated from 8 m DEM using a linear, unweighted Prewitt filter (Prewitt, 1970). A Kruskal-Wallis test finds out whether there is a significant difference in dead vegetation fraction between different slopes and aspect categories.

3. Results

As expected the reflectance values in the visible region of the spectrum steadily increased with increasing amounts of dead vegetation fraction present in the mixed pastures (Fig. 1a). In the visible region of the spectrum the reflectance was highest around 650 nm with the minimum around 400 nm. The samples with high dead vegetation content had lower reflectance values than those with low dead vegetation content in the NIR region of the spectrum. In the SWIR of the spectrum, around 1500 and 2000 nm the reflectance values steadily increased with increased dead vegetation content. The samples had a wide range of dead vegetation fractions (Fig. 1b) (CV = 49%), and the respective descriptive statistics of calibration and validation data sets are presented in Table 1.

3.1. Performance of vegetation indices for predicting the fraction of dead vegetation

Sequential linear regressions between all possible NDSVI band combinations produced from AisaFENIX data and real values of dead vegetation fraction were performed. The cross-validated regression results were presented in a 2-D correlation matrix visually highlighted with different colours corresponding to R^2 values. The matrix plot illustrates the R^2 values from 0 to 0.60, reflecting low to medium correlations, and the large number of bands with low R^2 values (Fig. 2). In Fig. 2, the spectral region around 1870 nm had the highest sensitivity to dead vegetation fraction changes. Of the full spectrum, the NDSVI with a combination of ρ_{1869} and ρ_{1886} showed the strongest correlation with the dead vegetation fraction (R^2_{CV} = 0.60, $RMSE_{CV}$ = 6.69, RPD_{CV} = 2.03). Using the calibration data a predictive equation was developed:

$$y_{Dvf} = 146.58 \times NDSVI_{1869-1886} + 37.328 \quad (9)$$

Where y_{Dvf} is the estimated dead vegetation fraction, $NDSVI_{1869-1886}$ is the *NDSVI* values derived from the derivative reflectance values at 1869 and 1886 nm using Eq. (1). The above model, when applied to validation data, yielded an R^2_P of 0.52, $RMSE_P$ of 7.38, and RPD_P of 1.77. The scatter graph of measured and predicted dead vegetation fraction is presented in Fig. 3a.

Similar to NDSVI, the SVI with a band combinations 1869 and 1886 nm yielded highest accuracy for predicting the dead vegetation fraction (R^2_{CV} = 0.58, $RMSE_{CV}$ = 6.81, RPD_{CV} = 2.00). However, the pattern of wavelength importance is different from the NDSVI pattern (Fig. 2).

$$y_{Dvf} = 74.581 \times SVI_{1869-1886} + 38.67 \quad (10)$$

Nevertheless, the performance of both models (NDVI and SR) was further degraded when applied on the external test data ($0.35 \le R^2 \le 0.36$) (Table 3).

Table 2
Cross-validated calibration data statistics for predicting dead vegetation fraction with different empirical methods.

Method	Number of bands	R^2_{CV}	$RMSE_{CV}$	RPD_{CV}
NDSVI	2	0.60	6.69	2.03
SVI	2	0.58	6.81	2.00
CAI	9	0.25	17.29	0.78
LCD	15	0.15	22.10	0.61
LCA	15	0.11	23.42	0.58
LCW	15	0.14	22.04	0.61
PLS	448	0.60	6.98	1.95
VIP-FiPLS	14	0.73	6.05	2.25

Table 3
Data statistics for predicting dead vegetation fraction with different empirical methods using test dataset obtained from second experiment.

Method	Number of bands	R^2	RMSE	RPD
NDVI	2	0.37	15.98	1.04
SVI	2	0.35	16.21	1.02
PLS	448	0.52	9.28	1.79
VIP-FiPLS	14	0.62	8.06	2.06

Using Eq. (3), a CAI model was developed from the calibration data which produced the lowest cross-validated coefficient of determination (R^2_{CV} = 0.25), the highest $RMSE_{CV}$ of 17.29, and the lowest RPD_{CV} of 0.78. The performance of the model was even lower on the validation data with a R^2_P = 0.15, $RMSE_P$ = 20.41, RPD_P = 0.63 (Fig. 3b).

Compared to all other indices lingo-cellulose indices (LCD, LCA and LCW) were performed poorly when estimating the fraction of dead vegetation ($0.11 \le R^2 \le 0.15$). Therefore, these indices were excluded from further evaluation.

3.2. Multivariate model

The cross-validated PLS model between pre-processed full-spectrum (448 bands) and estimated dead vegetation fraction yielded an accuracy of R^2_{CV} = 0.60, $RMSE_{CV}$ = 6.98, RPD_{CV} = 1.95 (Table 2). By using FiPLS the total number of variables (448) reduced significantly to 180, and highlighted important broad spectral regions across the spectrum. Using the VIP-FiPLS method, the number further reduced to 14 bands which were found to be highly relevant to the retrieval of the dead vegetation fraction. Overall, the feature selection based PLS model (VIP-FiPLS) offers a more accurate model (R^2_{CV} = 0.73, $RMSE_{CV}$ = 6.05, RPD_{CV} = 2.25) compared to models based on a full spectrum approach, optimized vegetation indices and CAI. The models developed on calibration data were applied on the validation data set (Fig. 3d). The models based on NDSVI, SVI and CAI performed poorly, indicating signs of instability. Despite the slight differences, the VIP-FiPLS model provided the best and most stable results on the validation data (R^2_P = 0.72, $RMSE_P$ = 6.2, RPD_P = 2.11). Important bands selected in the feature selection process are presented in Fig. 4. As can be seen, the blue and green regions of the visible spectrum, in NIR around 873 nm and the SWIR from 1460 to 1590 nm and from 1969 to 2400 nm were selected as important regions. The performance of both models including full spectrum and VIP-FiPLS were consistent on the test data, however, the prediction accuracy was slightly reduced (Table 3).

The calibration model based on VIP-FiPLS method was applied to the IS data of the farm obtained from AisaFENIX. Fig. 5 illustrates the fraction of dead vegetation across the farm with a wide range from 0% to 100%. The spatial distribution pattern of dead vegetation was distinctive. The central part of the farm (region C) exhibits lower proportion of dead vegetation and has less variability which was mainly due to the presence of new sown pasture. In region B of

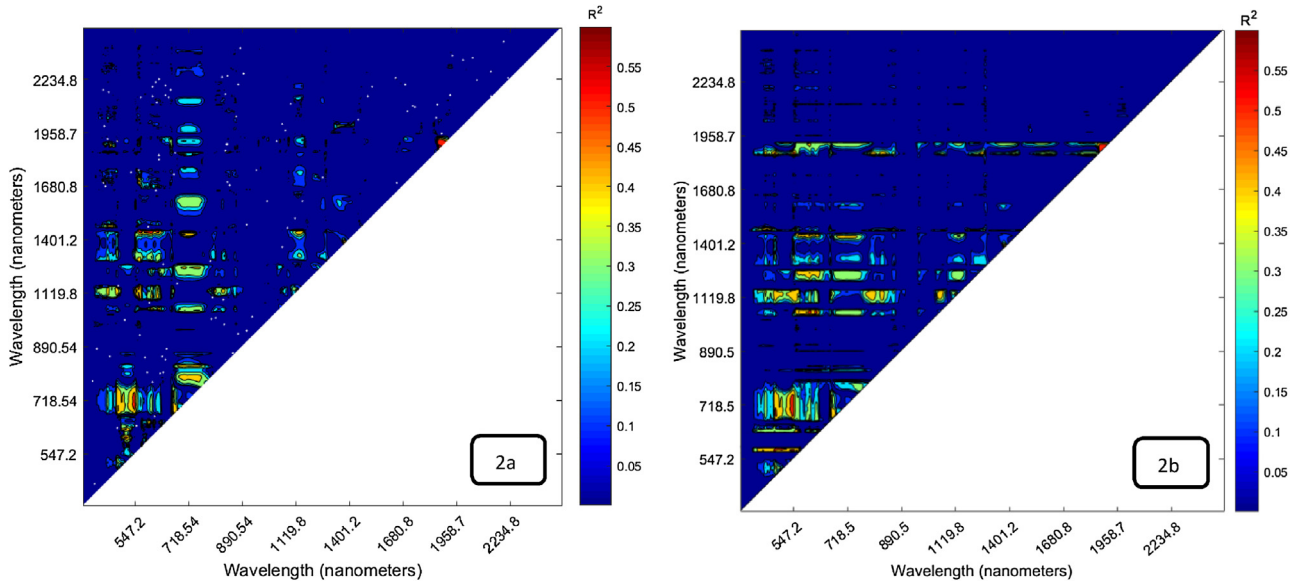

Fig. 2. 2-D correlation plot of R^2_{CV} values from a linear regression model using calibration data between measured dead vegetation fraction and all possible (a) NDSVI and (b) SVI combinations. The colour bar represents the scale of R^2 values of the plot.

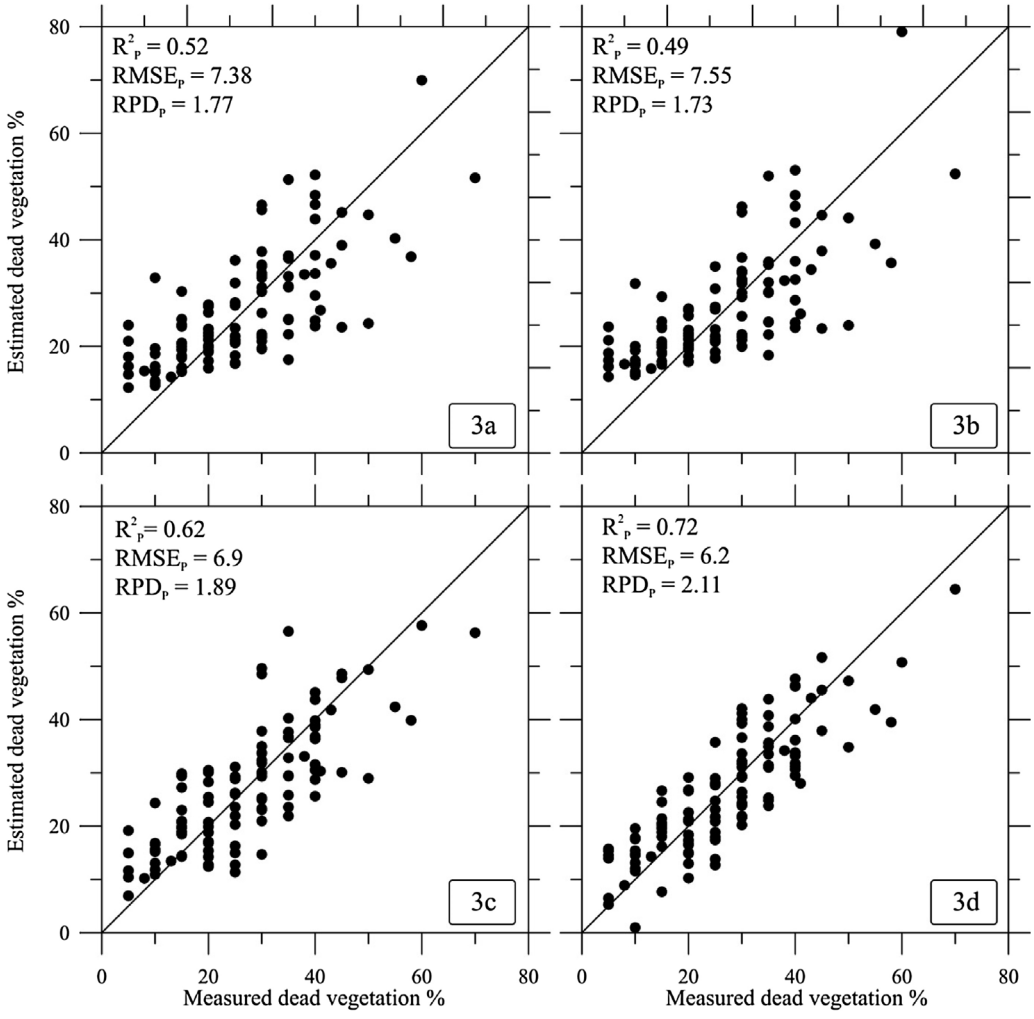

Fig. 3. Prediction of dead vegetation fraction from validation data using derivative reflectance values of (a) NDSVI (b) SVI (c) full spectrum PLS model (d) VIP-FiPLS model.

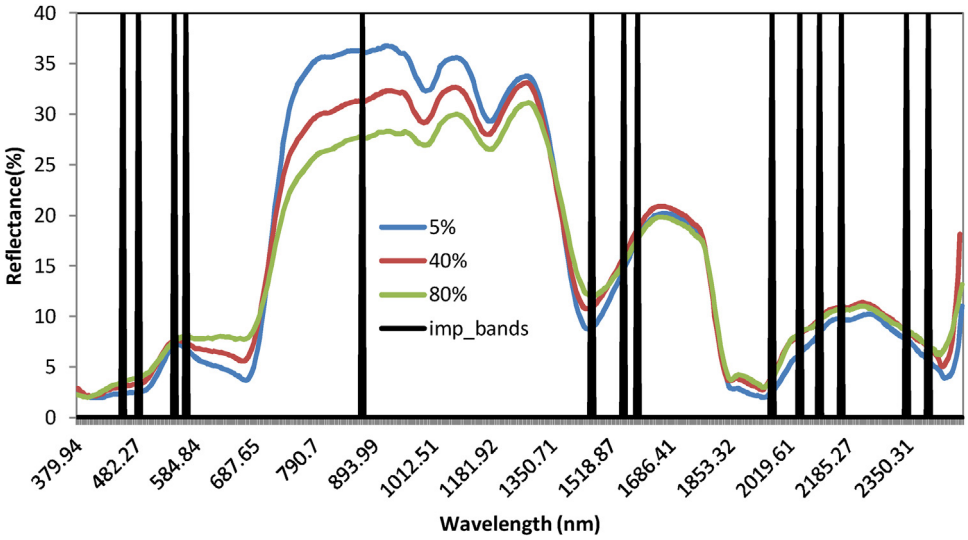

Fig. 4. Important bands (vertical lines) selected using forward interval partial least squares (FiPLS) for predicting dead vegetation fraction.

the farm, the dead vegetation fraction of mixed pastures was highly variable where the terrain slopes were high and older pasture was present. The predicted pixel-wise dead vegetation fraction values are presented in a histogram (Fig. 5D). The *y*-axis represents the frequency of dead vegetation fraction values and *x*-axis represents the absolute dead vegetation values. The histogram followed a normal distribution curve had a standard deviation of 11.7%, with the majority of the pixels (37%) containing 30% dead vegetation.

Based on the krus-wallis test, different terrain slope angles had a significant effect on dead vegetation fraction ($\chi^2 = 33.14$, df = 3, $p < 0.0001$). In contrast, different aspect categories had no significant effect on the content of dead vegetation ($\chi^2 = 8.72$, df = 3, $p = 0.084$) (Table 4). The results from the post-hoc test showed that the dead vegetation fraction on rolling to steep slopes slope-3 (16–25°) and slope-4 (>25°) was significantly higher than other slopes ($p < 0.05$). However, highest amount of dead vegetation fraction was recorded at steep slopes (slope-4; >25°). Under the North category, flat areas showed a significantly lower amount of dead vegetation than other slope categories ($p < 0.05$). In contrast, under East and West aspect categories, different slopes did not show any significant difference.

4. Discussion

The results indicate that high resolution airborne hyperspectral remote sensing has potential to estimate dead vegetation fraction in a mixed pasture environment. Changes in dead vegetation fraction have produced significant differences in the reflectance values particularly in the visible region (400–670 nm), near infrared region (790–1000 nm), and in discrete parts of the SWIR (1460–1520 nm; around 2000 nm). These observations had a comparable trend noticed by Xu et al. (2014) and Delegido et al. (2015). Typically, green vegetation has strong absorption features in the visible region due to the presence of chlorophyll pigments (Curran et al., 1997; Kokaly et al., 2009; Mutanga and Skidmore, 2004). Conversely, when vegetation starts senescence, chlorophyll denatures from the canopy which results in higher reflectance values. When the fraction of green vegetation is high, the SWIR is strongly influenced by water absorptions hence low reflectance was noticed (Fig. 1a). In contrast, dead vegetation has low water content therefore high reflectance was seen in dead vegetation dominant samples (Fig. 1). Compared to conventional multispectral sensors, the hyperspectral sensor has an improved capability as it holds contiguous narrow bands to distinguish subtle absorption features of all types of vegetation which minimizes the problem of spectral ambiguity between dead vegetation and soil (Li and Guo, 2015). In this research it has been proven that the dead vegetation fraction could be estimated with high accuracy.

Researchers have attempted to develop vegetation indices for estimating the dead vegetation fraction but with limited success in mixed pasture due to complex environments (Ren and Zhou, 2012; Xu et al., 2014). The 2D correlation plot (Fig. 2) highlights the importance of narrow band vegetation indices from the SWIR region (around 1870 nm) for estimating the dead vegetation fraction, as such, SWIR has strong discriminative ability between dead vegetation, green vegetation and soil (Daughtry et al., 2004). However, vegetation indices failed to predict the fraction of dead vegetation on the test data, indicating its unreliability for quantitative analysis. In this study, all SWIR based indices such as NDSVI, SVI, ligno-cellulose absorption indices and CAI failed to predict dead vegetation fraction. This might be due to the abundance of water in green vegetation which inhibits the relationship (Kokaly and Clark, 1999; Nagler et al., 2003). The above mentioned indices were developed from agriculture crops where cellulose and lignin concentrations are high with strong absorption peaks, thus these indices worked well. In contrast, mixed pastures contain low concentrations of cellulose and lignin, hence weak spectral absorptions could be expected. Moreover, soil mineral absorption features around 2200 nm may have affected the relationship between CAI and the dead vegetation fraction (Daughtry et al., 2010; Nagler et al., 2003). The presence of green vegetation influences the performance of CAI, and it is worse when the fraction of green vegetation is more than 30% (Daughtry et al., 2004; Li and Guo, 2015). Mixed species with different canopy structures also significantly influence the relationship between the CAI and NPV (Numata et al., 2008). It is surprising that the full spectrum PLS model yielded reasonable accuracy compared to optimized vegetation indices. However, the performance of the full spectrum model was consistent over the independent test data (Table 3). This might be because the full spectrum comprises sufficient information for discriminating dead vegetation from other properties (Numata et al., 2008).

Using feature selection algorithms that included only the best bands in the PLS model significantly improved the prediction performance over full spectrum and vegetation indices approaches. This highlights that selecting spectral bands which are highly relevant to the variable of interest significantly improves the accuracy

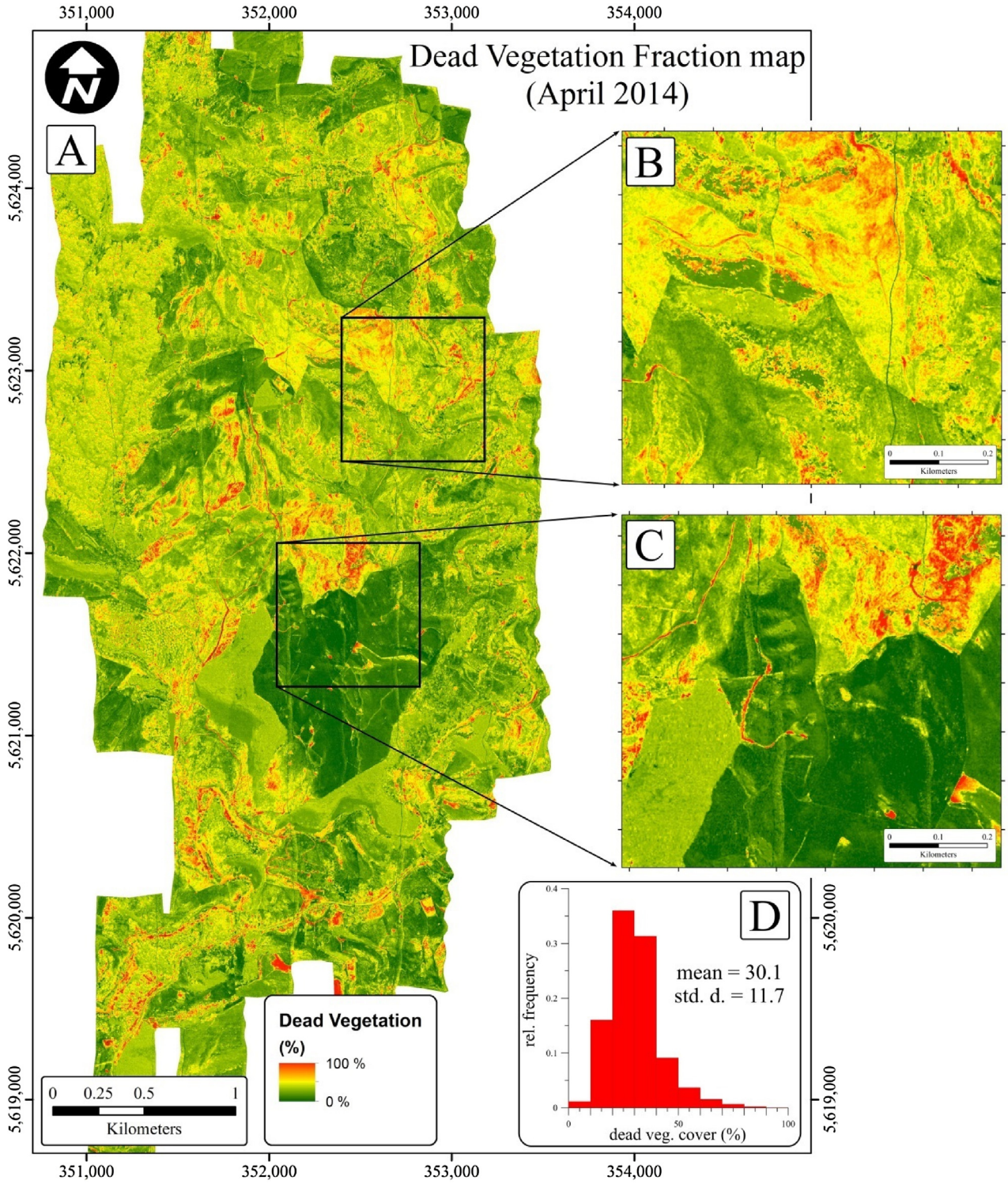

Fig. 5. Pixel based dead vegetation fraction spatial map derived using hyperspectral image from AisaFENIX.

Table 4
Mean values of dead vegetation fraction in mixed pastures under different slope and aspect categories. Statistical test was performed using Kruskal-Wallis test followed by post-hoc test for multiple comparisons.

Slope-1 (0–8°)	Slope-2 (8–16°)	Slope-3 (16–25°)	Slope-4 (>25°)	Aspect	Significance
24.95b	28.63b	32.08a	38.96a	All aspects	$\chi2 = 33.14$, df = 3, $p < 0.0001$
19b	29.44ab	38.37a	44.66a	North	$\chi2 = 17.53$, df = 3, $p < 0.001$
23.42b	25.93b	25.9b	38a	South	$\chi2 = 27.88$, df = 3, $p < 0.001$
26.77	33.8	31.8	34.5	East	$\chi2 = 6.24$, df = 3, $p = 0.1003$
32.53	31.14	30	36.5	West	$\chi2 = 1.46$, df = 2, $p = 0.4812$

Means followed by different letters in each row are statistically significant.

of the model (Feilhauer et al., 2015). Moreover, the model had excellent generalization ability with consistent performance on the different datasets, though the accuracy was slightly reduced on test data. This indicates appropriate bands, which hold sufficient information, were selected for prediction of the fraction dead vegetation. It is likely that irrelevant bands and other noisy bands cause disturbances in the relationships of the estimates (Inoue et al., 2012). Each feature selection method has issues in selecting the appropriate and stable bands to provide accurate and improved results; hence we combined iterated FiPLS and VIP to achieve better accuracy. The selected bands present in the visible region related to the absorption of pigments (Gitelson et al., 2006), and the absorption around 1460 nm related to water (Curran, 1989). The selected bands in the SWIR played a key role in improving the prediction accuracy (Fig. 4) where three broad absorption features around 1730, 2100 and 2300 nm are primarily associated with nitrogen, cellulose and lignin (Curran, 1989; Daughtry et al., 2010; Kokaly and Clark, 1999). Absorption at 1730 nm is specifically associated with C—H stretch due to cellulose and lignin (Curran, 1989). The band at 2100 nm is attenuated with cellulose which is absent in spectra of soil and green vegetation (Daughtry et al., 2004). The absorption around 2300 is caused by C—H stretch of cellulose and nitrogen (Curran, 1989). This indicates that absorption features in the SWIR are important for estimating the dead vegetation fraction in mixed pastures. The combination of these spectral features helped to improve the estimation accuracy of dead vegetation fraction. Numata et al. (2008) indicated that combining senescent indices and water absorption bands may improve the relationships between spectral data and the content of NPV.

Generally, dead vegetation accumulation is high during summer and autumn, and contains high concentrations of liginin, cellulose and hemicellulose compared to green vegetation (Litherland et al., 2002). This supports our results as the experiment which was conducted in autumn had higher dead vegetation accumulation. The method can be extended to a larger scale by using the data from future space missions such as Environmental Mapping and Analysis Programme (EnMAP), and Hyperspectral Infrared Imager (HyspIRI) where it routinely samples the land surfaces in the SWIR of the electromagnetic spectrum (Roberts et al., 2012; Stuffler et al., 2007).

A possible reason for some of the error in the model was the scale of the ground sampling that did not exactly match the pixel resolution. The dead vegetation fraction has high spatial heterogeneity which may not have been adequately accounted for in the smaller quadrat size compared to the pixel resolution. In this study we used 0.25 m^2 plots for ground sampling. The relative pixel size collected from the sensor was $3 \times 3\,m^2$ which could have introduced error in the model. Another possible reason is that in the longer wavelength region (2300–2400 nm) the absorptions caused by 2nd overtone, which is less intense, may be masked by sensor noise (Curran, 1989). Moreover, the mixed scenes have spectra from green and dead vegetation where green vegetation spectra might attenuates the signal from the dead vegetation.

A wide range of variability of dead vegetation fraction was visible in Fig. 5 caused by topographical factors, environmental factors and animal interactions (Gillingham, 1973). Statistical analysis confirmed that the dead vegetation fraction was significantly higher on steeper slopes (>25°) than on other slopes. This may be attributable to a lower availability of water in soil, greater runoff on steeper slopes and lower soil fertility due to increased nutrient transfer to flats (Gillingham, 1973).

5. Conclusion

Accurate assessment of the dead vegetation fraction is critical for pasture management in order to improve farm profitability by providing high quality feed for animals to improve animal perforamnce. The study demonstrated the retrieval of the dead vegetation fraction in mixed pastures from imaging spectroscopy data obtained from AisaFENIX using different empirical approaches. All vegetation indices failed to predict dead vegetation fraction. However, the feature selection based PLS model estimated dead vegetation fraction with high accuracy, and reasonable performance was shown on the external test data. The wavebands selected in the model for predicting the dead vegetation fraction were located in visible and SWIR regions of the spectrum. A total of 14 bands were found as most relevant to dead vegetation changes. Slope angle had a significant impact on the accumulation of the dead vegetation fraction; steep slopes had high amounts of dead vegetation compared to other slopes.

Acknowledgments

This study was financially supported by Ministry of Primary Industries (MPI) and Ravensdown Limited, New Zealand as part of the Primary Growth Partnership (PGP) project, pioneering to precision application of fertiliser on hill country. The authors thank the field team Pip McVeagh, Tommy Cushnahan, Ina Draganova, Eduardo Sandoval and Kate Saxton from Massey University, and the field team from AgResearch, Ruakura Research Centre, Hamilton, led by Mr Grant Rennie. The authors also gratefully acknowledge the cooperation of Atihau Whanganui Corporation for giving access to the Ohorea station.

References

Abdi, H., Williams, L., 2010. Jackknife. Encyclopedia of Research Design. Sage, Thousand Oaks, CA, pp. 655–660.
Andersen, C.M., Bro, R., 2010. Variable selection in regression—a tutorial. J. Chemom. 24, 728–737.
Asner, G.P., Borghi, C.E., Ojeda, R.A., 2003. Desertification in central Argentina: changes in ecosystem carbon and nitrogen from imaging spectroscopy. Ecol. Appl. 13, 629–648.
Curran, P.J., Kupiec, J.A., Smith, G.M., 1997. Remote sensing the biochemical composition of a slash pine canopy. IEEE Trans. Geosci. Remote Sens. 35, 415–420.
Curran, P.J., 1989. Remote sensing of foliar chemistry. Remote Sens. Environ. 30, 271–278.
Daughtry, C., McMurtrey III, J., Chappelle, E., Hunter, W., Steiner, J., 1996. Measuring crop residue cover using remote sensing techniques. Theor. Appl. Climatol. 54, 17–26.
Daughtry, C.S.T., Hunt Jr., E.R., McMurtrey Iii, J.E., 2004. Assessing crop residue cover using shortwave infrared reflectance. Remote Sens. Environ. 90, 126–134.
Daughtry, C.S.T., Serbin, G., Reeves, J., Doraiswamy, P., Hunt, E.R., 2010. Spectral reflectance of wheat residue during decomposition and remotely sensed estimates of residue cover. Remote Sens. 2, 416.
Daughtry, C.S., 2001. Discriminating crop residues from soil by shortwave infrared reflectance. Agron. J. 93, 125–131.
Delegido, J., Verrelst, J., Rivera, J.P., Ruiz-Verdú, A., Moreno, J., 2015. Brown and green LAI mapping through spectral indices. Int. J. Appl. Earth Obs. Geoinf. 35 (Part B), 350–358.
Feilhauer, H., Asner, G.P., Martin, R.E., 2015. Multi-method ensemble selection of spectral bands related to leaf biochemistry. Remote Sens. Environ. 164, 57–65.
Gillingham, A., 1973. Influence of physical factors on pasture growth on hill country. Proc. N. Z. Grassl. Assoc., 77–85.
Giraudoux, P., 2012. pgirmess: Data analysis in ecology, R package version, 1.6.2 ed, Available at the following web site: http://giraudoux.pagesperso-orange.fr/.
Gitelson, A.A., Keydan, G.P., Merzlyak, M.N., 2006. Three-band model for noninvasive estimation of chlorophyll, carotenoids, and anthocyanin contents in higher plant leaves. Geophys. Res. Lett. 33, 111402.
Guerschman, J.P., Hill, M.J., Renzullo, L.J., Barrett, D.J., Marks, A.S., Botha, E.J., 2009. Estimating fractional cover of photosynthetic vegetation, non-photosynthetic vegetation and bare soil in the Australian tropical savanna region upscaling the EO-1 Hyperion and MODIS sensors. Remote Sens. Environ. 113, 928–945.
Hestir, E.L., Khanna, S., Andrew, M.E., Santos, M.J., Viers, J.H., Greenberg, J.A., Rajapakse, S.S., Ustin, S.L., 2008. Identification of invasive vegetation using hyperspectral remote sensing in the California Delta ecosystem. Remote Sens. Environ. 112 (11), 4034–4047.
Holmes, C.W., Wilson, G.F., Mackenzie, D.D.S., Flux, D.S., Brookes, I.M., Davey, A.W.F., 2007. Milk Production from Pasture. Massey University, Palmerston North, New Zealand.

Inoue, Y., Sakaiya, E., Zhu, Y., Takahashi, W., 2012. Diagnostic mapping of canopy nitrogen content in rice based on hyperspectral measurements. Remote Sens. Environ. 126, 210–221.
Keogh, R., 1986. Fungal distribution and livestock defoliation patterns in pasture ecosystems, and the development and control of dietary-dependent disorders. Proc. N. Z. Grassl. Assoc., 93–98.
Knox, N.M., Skidmore, A.K., Prins, H.H.T., Asner, G.P., van der Werff, H.M.A., de Boer, W.F., van der Waal, C., de Knegt, H.J., Kohi, E.M., Slotow, R., Grant, R.C., 2011. Dry season mapping of savanna forage quality, using the hyperspectral Carnegie Airborne Observatory sensor. Remote Sens. Environ. 115, 1478–1488.
Kokaly, R.F., Clark, R.N., 1999. Spectroscopic determination of leaf biochemistry using band-depth analysis of absorption features and stepwise multiple linear regression. Remote Sens. Environ. 67, 267–287.
Kokaly, R.F., Asner, G.P., Ollinger, S.V., Martin, M.E., Wessman, C.A., 2009. Characterizing canopy biochemistry from imaging spectroscopy and its application to ecosystem studies. Remote Sens. Environ. 113 (Supplement 1), S78–S91.
Landmann, T., Piiroinen, R., Makori, D.M., Abdel-Rahman, E.M., Makau, S., Pellikka, P., Raina, S.K., 2015. Application of hyperspectral remote sensing for flower mapping in African savannas. Remote Sens. Environ. 166, 50–60.
Li, Z., Guo, X., 2015. Remote sensing of terrestrial non-photosynthetic vegetation using hyperspectral, multispectral, SAR, and LiDAR data. Prog. Phys. Geogr. 40, 276–304, 0309133315582005.
Litherland, A.J., Woodward, S.J.R., Stevens, D.R., McDougal, D.B., Boom, C.J., Knight, T.L., Lambert, M.G., 2002. Seasonal variations in pasture quality on New Zealand sheep and beef farms. Proc. N. Z. Soc. Anim. Prod. 62, 138–142.
Morris, C.A., Towers, N.R., Hohenboken, W.D., Maqbool, N., Smith, B.L., Phua, S.H., 2004. Inheritance of resistance to facial eczema: a review of research findings from sheep and cattle in New Zealand. N. Z. Vet. J. 52, 205–215.
Mutanga, O., Skidmore, A.K., 2004. Integrating imaging spectroscopy and neural networks to map grass quality in the Kruger National Park, South Africa. Remote Sens. Environ. 90, 104–115.
Nagler, P.L., Inoue, Y., Glenn, E.P., Russ, A.L., Daughtry, C.S.T., 2003. Cellulose absorption index (CAI) to quantify mixed soil–plant litter scenes. Remote Sens. Environ. 87, 310–325.
Norgaard, L., Saudland, A., Wagner, J., Nielsen, J.P., Munck, L., Engelsen, S.B., 2000. Interval Partial Least-Squares Regression (iPLS): A comparative chemometric study with an example from near-infrared spectroscopy. Appl. Spectrosc. 54, 413–419.
Numata, I., Roberts, D.A., Chadwick, O.A., Schimel, J.P., Galvão, L.S., Soares, J.V., 2008. Evaluation of hyperspectral data for pasture estimate in the Brazilian Amazon using field and imaging spectrometers. Remote Sens. Environ. 112, 1569–1583.
Prewitt, J.M., 1970. Object enhancement and extraction. Picture Processing and Psychopictorics, vol. 10., pp. 15–19.
Pullanagari, R., Yule, I., Tuohy, M., Hedley, M., Dynes, R., King, W., 2012. In-field hyperspectral proximal sensing for estimating quality parameters of mixed pasture. Precis. Agric. 13, 351–369.
Qi, J., Wallace, O., 2002. Biophysical attributes estimation from satellite images in arid regions. In: Geoscience and Remote Sensing Symposium, 2002. IGARSS'02. 2002 IEEE International, IEEE, pp. 2000–2002.
Qi, J., Marsett, R., Heilman, P., Bieden-bender, S., Moran, S., Goodrich, D., Weltz, M., 2002. RANGES improves satellite-based information and land cover assessments in southwest United States. Eos Trans. Am. Geophys. Union 83, 601–606.
Ren, H., Zhou, G., 2012. Estimating senesced biomass of desert steppe in Inner Mongolia using field spectrometric data. Agric. For. Meteorol. 161, 66–71.
Ren, H., Zhou, G., Zhang, F., Zhang, X., 2012. Evaluating cellulose absorption index (CAI) for non-photosynthetic biomass estimation in the desert steppe of Inner Mongolia. Chin. Sci. Bull. 57, 1716–1722.
Richter, R., Schläpfer, D., 2014. Atmospheric/Topographic Correction for Airborne Imagery, ATCOR-4 User Guide, DLR Report DLR-IB 565-02/14. DLR German Aerospace Centre, Wessling, Germany.
Roberts, D.A., Quattrochi, D.A., Hulley, G.C., Hook, S.J., Green, R.O., 2012. Synergies between VSWIR and TIR data for the urban environment: an evaluation of the potential for the Hyperspectral Infrared Imager (HyspIRI) decadal survey mission. Remote Sens. Environ. 117, 83–101.
Siegel, S., Castellan, N.J., 1956. Nonparametric Statistics for the Behavioral Sciences. McGraw-Hill, New York.
Skidmore, A.K., Ferwerda, J.G., Mutanga, O., Van Wieren, S.E., Peel, M., Grant, R.C., Prins, H.H.T., Balcik, F.B., Venus, V., 2010. Forage quality of savannas—simultaneously mapping foliar protein and polyphenols for trees and grass using hyperspectral imagery. Remote Sens. Environ. 114, 64–72.
Stuffler, T., Kaufmann, C., Hofer, S., Förster, K., Schreier, G., Mueller, A., Eckardt, A., Bach, H., Penne, B., Benz, U., 2007. The EnMAP hyperspectral imager—an advanced optical payload for future applications in Earth observation programmes. Acta Astronaut. 61, 115–120.
Ustin, S.L., Valko, P.G., Kefauver, S.C., Santos, M.J., Zimpfer, J.F., Smith, S.D., 2009. Remote sensing of biological soil crust under simulated climate change manipulations in the Mojave Desert. Remote Sens. Environ. 113, 317–328.
White, J., Hodgson, J., 2000. New Zealand Pasture and Crop Science. Oxford University Press.
Wold, S., Sjöström, M., Eriksson, L., 2001. PLS-regression: a basic tool of chemometrics. Chemom. Intell. Lab. Syst. 58, 109–130.
Xu, D., Guo, X., Li, Z., Yang, X., Yin, H., 2014. Measuring the dead component of mixed grassland with Landsat imagery. Remote Sens. Environ. 142, 33–43.
Yang, X., Guo, X., 2014. Quantifying responses of spectral vegetation indices to dead materials in mixed grasslands. Remote Sens. 6, 4289–4304.
Zhang, B., Valentine, I., Kemp, P., 2004. Modelling hill country pasture production: a decision tree approach. Proc. N. Zeal. Soc. Anim Prod., 197–201.
Zou, X., Zhao, J., Li, Y., 2007. Selection of the efficient wavelength regions in FT-NIR spectroscopy for determination of SSC of 'Fuji' apple based on BiPLS and FiPLS models. Vib. Spectro. 44, 220–227.